


Angular behavior of flux dynamics in YBCO films with crossed columnar defects around the *ab*-plane

Tetsuro Sueyoshi¹ , Yuichi Furuki¹, Takanori Fujiyoshi¹,
Fumiaki Mitsugi¹, Tomoaki Ikegami¹, Ataru Ichinose² and Norito Ishikawa³

¹ Faculty of Advanced Science and Technology, Kumamoto University, 2-39-1 Kurokami, Chuo-ku, Kumamoto 860-8555, Japan

² Central Research Institute for Electric Power Industry, Nagasaka, Yokosuka, Kanagawa 240-0196, Japan

³ Japan Atomic Energy Agency (JAEA), Tokai-mura, Ibaraki 319-1195, Japan

E-mail: tetsu@cs.kumamoto-u.ac.jp

Received 26 June 2018, revised 17 September 2018

Accepted for publication 21 September 2018

Published 18 October 2018



Abstract

We systematically investigated the influence of columnar defects (CDs) on the flux dynamics around $B \parallel ab$ in $\text{YBa}_2\text{Cu}_3\text{O}_{7-\delta}$ (YBCO) films, where two types of the crossed CD configurations with the crossing angle relative to the c -axis, $\theta_i = \pm 30^\circ$ and $\pm 60^\circ$, were prepared by using 200 MeV Xe ion irradiation. The crossed CDs with $\theta_i = \pm 30^\circ$ induce a peak of critical current density J_c centered at $B \parallel c$, which suggests a typical entanglement state of flux lines. The J_c at $B \parallel ab$, by contrast, is insensitive to the crossed CDs with $\theta_i = \pm 60^\circ$, which are crossing at $\pm 30^\circ$ around the ab -plane. In addition, the behaviors of the glass–liquid transition temperature T_g and the dynamic critical exponent z indicate that the VG state develops at $B \parallel ab$ not only for $\theta_i = \pm 30^\circ$ but also for $\theta_i = \pm 60^\circ$. The difference in the contribution of CDs to the flux dynamics for between $\theta_i = \pm 30^\circ$ and $\pm 60^\circ$ also stands out at $B \parallel$ CDs, where the magnetic field for $\theta_i = \pm 60^\circ$ is more tilted toward the ab -plane: the J_c peak at $B \parallel$ CDs occurs in any magnetic field for $\theta_i = \pm 60^\circ$, whereas the correlated pinning state disappears in high magnetic fields for $\theta_i = \pm 30^\circ$. These results suggest that the pinning by CDs is angle-dependent due to the flux line structure with strong line tension around $B \parallel ab$: CDs around the ab -plane can trap flux lines along their long axis only in much narrower angular-range, in comparison with CDs around the c -axis.

Keywords: high- T_c superconductors, critical current density, flux pinning, columnar defects, anisotropy

(Some figures may appear in colour only in the online journal)

1. Introduction

A notable feature of critical current density J_c in high- T_c superconductors is to exhibit a large anisotropy against a magnetic field orientation, resulting in the obstacle to superconducting magnet applications using $\text{REBa}_2\text{Cu}_3\text{O}_y$ (REBCO, RE: rare earth element) coated conductors: a minimum in the angular variation of J_c , which is usually exhibited at $B \parallel c$, limits the amplitude of the operation current. The anisotropy in J_c arises from the electronic mass

anisotropy in the layered structure composed of CuO_2 planes defining the crystallographic ab -plane [1]. One of the promising ways to overcome the intrinsic nature in the J_c is the tuning of flux pinning landscape, where additional crystalline defects and impurities are installed as pinning centers (PCs) [2, 3]: it is essential for the improvement of the J_c anisotropy that flux line dynamics is controlled with PCs suitable for each direction of magnetic field.

Columnar defects (CDs) [4] and dislocations [5], which belong to one-dimensional (1D) PCs, strongly trap flux lines

Table 1. Samples in this work.

Sample	Crossing angle of CDs relative to c -axis, θ_i	B_ϕ (T)	T_c (K)	J_{c0} (MA cm $^{-2}$)
Cr30	$\pm 30^\circ$	3	87.9	2.3
Cr60	$\pm 60^\circ$	3	86.7	0.87

all along their long axis. Then, the 1D-PCs form a so-called Bose-glass (BG) state [6], where the motion of flux lines is more suppressed than the case of a vortex glass (VG) phase induced by point defects [7]. Hence, 1D-PCs are usually introduced along the c -axis for the purpose of the reduction of the J_c anisotropy. The flux pinning by 1D-PCs, moreover, can provides a variety of pinning manner according to their configurations such as the dispersion (splay) in their directions: the small dispersion enhances the flux pinning especially at the mid direction of the dispersion (usually at the c -axis direction), forming a splay glass (SG) state [8]; the larger dispersion pushes up the J_c over a wider angular range of magnetic field [9, 10]. Tuning of the dispersion in the direction of 1D-PCs may exert the effective pinning of 1D-PCs not only at $B \parallel c$ but also in all directions of magnetic field, making the J_c fairly isotropic [11].

The anisotropic layered structure in high- T_c materials, on the other hand, provides different structures of flux lines depending on the direction of magnetic field. That is, flux lines with an elliptical core are formed in a magnetic field tilted toward the ab -plane, whereas the flux lines have a circular core as conventional Abrikosov vortices at $B \parallel c$ [1]. Moreover, the continuous vortex structure under the tilted magnetic field crosses over into a kinked vortex structure consisting of pan-cake vortices and Josephson vortex segments below a certain temperature, T_{cr} [12]: the magnetic field component parallel to the ab -plane for the tilted flux lines is localized between CuO_2 layers, i.e. the Josephson vortex segments appears. Such an angle-dependent structure of flux lines significantly affects the flux pinning behaviors: the elliptical core shape of flux lines can provide a broad J_c peak centered at the c -axis in moderate magnetic fields at higher temperatures in YBCO films containing relatively large nanoparticles ($>2\xi$, ξ : coherence length) [13]; an inverse correlation between J_c and n -values in $E \sim J^n$ (E and J are electrical field and current density) at $B \parallel ab$, where a sharp J_c peak is accompanied by a rapid drop of the n -values, is a sign of the formation of the kinked vortex structure at lower temperatures [14, 15]. The pinning interaction between the angle-dependent structure of flux lines and tilted or direction-dispersed 1D-PCs, on the other hand, has not been well studied so far, even though there have been a lot of studies on the flux pinning by 1D-PCs in high- T_c materials, which have focused on the flux pinning for Abrikosov vortices around $B \parallel c$ in most cases.

Recently, we reported the influence of crossed CDs on J_c at $B \parallel ab$ as a function of the crossing angle of CDs, where the CDs were introduced by heavy-ion beams tilted with respect to the ab -plane in GdBCO coated conductors [16, 17]. It was demonstrated that crossed CDs are hard to increase the

J_c at $B \parallel ab$, even though the crossing angle is relatively low with respect to the ab -plane. This implies that crossed CDs or tilted CDs do not always induce the SG state or the BG one for the angle-dependent structure of flux lines in any direction of magnetic field.

In this work, we systematically investigated the angular behaviors of the vortex state in YBCO films with crossed CDs around the ab -plane, where two type of the crossing angle with respect to the c -axis, $\theta_i = \pm 30^\circ$ and $\pm 60^\circ$, were prepared by using 200 MeV Xe ion irradiation: the vortex state behavior is an indicator exhibiting which kind of PCs is dominant in a certain magnetic field direction, by which we can clarify whether CDs work as effective PCs for the angle-dependent structure of flux lines in a certain direction of magnetic field. The nature of the glass state and the liquid one at between $B \parallel c$ and $B \parallel ab$ was examined through the angular dependence of J_c and flux flow resistivity ρ , respectively. Moreover, the glass–liquid transition temperature T_g and the dynamic critical exponent z were estimated from the critical scaling behavior of E – J characteristics, in order to clarify the ground states of flux lines at $B \parallel c$, at $B \parallel$ CDs, and at $B \parallel ab$. On the basis of the flux dynamics ranging from the glass state to the liquid one via the glass–liquid transition, we attempted to reveal the pinning mechanism of CDs for the angle-dependent structure of flux lines, especially with a focus on the vortex state around $B \parallel ab$.

2. Experimental details

The samples in this work were c -axis oriented YBCO thin films, which were fabricated by a pulsed laser deposition technique on (100) surface of SrTiO_3 single crystal substrates. The thickness of the films was about 300 nm. The films were patterned into a bridge geometry with about 40 μm width and 1 mm length before the irradiation.

The irradiation with 200 MeV Xe ions was performed at room temperature using a tandem accelerator at JAEA in Tokai, Japan. To install crossed CDs, the incident ion beam was tilted off the c -axis by $\pm\theta_i$ and was always directed perpendicular to the bridge direction of the sample. We prepared two kinds of the CD crossing angle, $\theta_i = \pm 30^\circ$ and $\pm 60^\circ$, where the latter provides the configuration of CDs crossing at $\pm 30^\circ$ relative to the ab -plane. The total planar density of CDs, which is defined with respect to the c -axis, corresponds to a dose equivalent matching field $B_\phi = 3$ T. The samples were irradiated with a half of the total fluence in each direction of the irradiation. Note that the fluence of the irradiation differs according to the irradiation angle by $1/\cos \theta_i$: the total fluences in the plane perpendicular to the

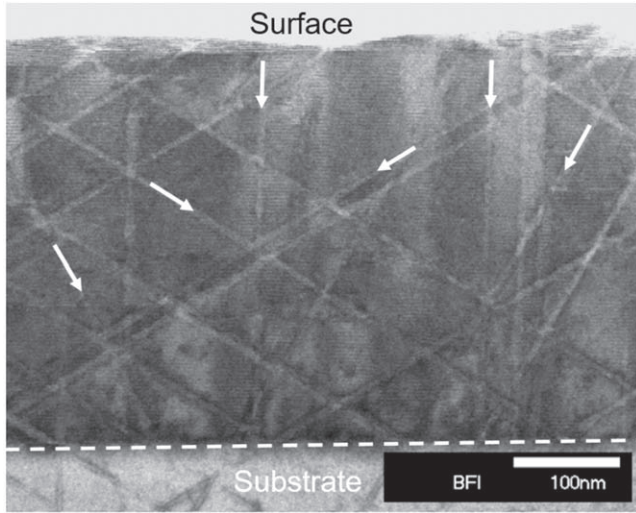


Figure 1. Bright field TEM image showing the CDs in various directions, $\theta_i = 0^\circ, \pm 30^\circ$, and $\pm 60^\circ$, which are installed in a YBCO thin film by 200 MeV Xe ion irradiation. The arrows indicate several ion tracks.

beam are 1.68×10^{11} ions cm^{-2} for $\theta_i = \pm 30^\circ$ and 2.90×10^{11} ions cm^{-2} for $\theta_i = \pm 60^\circ$, respectively. The ion-beam current was set to about 5 nA to avoid heating of the samples by the high-energy irradiation, where the irradiation time was about 43 s per fluence of 1.0×10^{11} ions cm^{-2} . Table 1 represents the specifications of the samples used in this work (T_c : critical temperature, J_{c0} : self-field critical current density at 77.3 K. The two parameters were estimated from transport measurements, where the value of T_c was defined as the temperature at which electrical resistivity became below $2 \times 10^{-3} \mu\Omega \text{ cm}$ and the value of J_{c0} was determined using a criterion of electrical field, $1 \mu\text{V cm}^{-1}$). The low T_c and the low J_{c0} for Cr60 are due to the net irradiation damage, which is simply proportional to the fluence of the irradiation: the total fluence in the plane perpendicular to the ion-beam is 2.90×10^{11} ions cm^{-2} for Cr60, which is roughly twice as compared with Cr30.

For the oblique irradiations with $\theta_i = \pm 60^\circ$, the projectile range in the film is more elongated, where the electronic stopping power S_e changes from 2.8 to $2.1 \text{ keV } \text{\AA}^{-1}$ through the superconducting film. As the threshold value of S_e for CD formation is $2.0 \text{ keV } \text{\AA}^{-1}$ [18], the formation of continuous CDs can be expected through the superconducting film. Figure 1 shows a cross-sectional transmission electron microscopy image of a YBCO thin film with CDs inclined at $\theta_i = 0^\circ, \pm 30^\circ$, and $\pm 60^\circ$, which was prepared to check the morphology of CDs produced by the 200 MeV Xe ion irradiation. It is found that the straight and continuous CDs completely penetrate the superconducting film from the surface to the bottom along the irradiation direction for any irradiation angle. The diameter of CDs is almost constant, i.e. 5–9 nm, regardless of the irradiation angle or the depth position, which roughly coincides with CD diameters for $S_e \sim 2.8 \text{ keV } \text{\AA}^{-1}$ in previous reports [18, 19].

The transport properties were measured using a four-probe method, where magnetic field was applied always

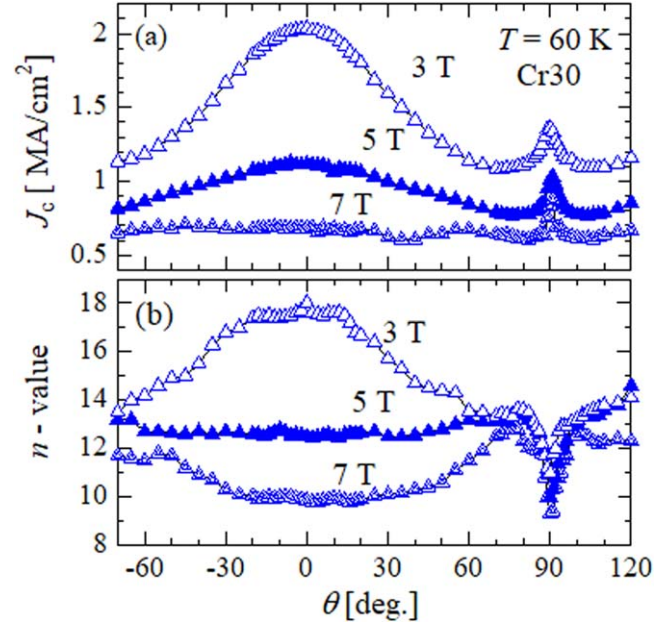


Figure 2. Angular dependence of (a) critical current density J_c and (b) n -value at 60 K for various magnetic fields in YBCO films with (a) $\theta_i = \pm 30^\circ$, Cr30.

perpendicular to the transport current direction (maximum Lorentz force configuration). For the transport measurements as a function of applied magnetic field direction, the sample was rotated to set various angles θ between the c -axis and the magnetic field. Angular dependence of flux flow resistivity ρ was measured with transport current density of about 30 A cm^{-2} . To evaluate the behaviors of the glass–liquid transition in various magnetic fields, a series of E – J curves as a function of temperatures were measured at $B \parallel c$, $B \parallel$ CDs, and $B \parallel ab$. We paid attention especially to the stability of the temperature during the measurements, which was better than $\pm 0.02 \text{ K}$. It should be noted that estimating T_g and z from scaling analysis of E – J curves has always been a controversial procedure, since the scaling analysis is too flexible to determine the absolute values of T_g and z without ambiguity [20, 21]. In this work, we discuss the nature of the vortex state not through the absolute values but through the relative differences in the magnetic field dependences of T_g and z .

3. Results and discussion

Figure 2 shows the angular dependence of J_c and n -value at 60 K in magnetic fields up to 7 T for YBCO films with $\theta_i = \pm 30^\circ$, which enables us to discuss the influence of the crossed CDs on the glass state in various magnetic field orientations. The n -value is extracted from a linear fit to empirical electric field (E) versus current density (J) relation $E \sim J^n$ in the range of 1 – $10 \mu\text{V cm}^{-1}$, where the n -value is equivalent to $U_0/k_B T$ (U_0 : pinning potential energy) [14, 22], reflecting thermal activation for flux motion. Focusing on the behaviors of J_c around $B \parallel c$, a broad peak centered at $\theta = 0^\circ$ can be observed at 3 T for both the J_c and the n -value. The

accommodation angle θ_a , at which the J_c and the n -value show the minimum, is approximately 70° . This suggests that the crossed CDs interact with flux lines in a wide angular-range. Previously, we reported that the additional peak of J_c emerges around $B \parallel c$ when the crossing angle of CDs relative to the c -axis is smaller than $\pm 45^\circ$ for YBCO films: CDs tilted at $\theta_i < 45^\circ$ can trap flux lines partially along their long axis, inducing entanglement of the flux lines on the crossed CDs [10]. Therefore, the crossed CDs with $\theta_i = \pm 30^\circ$ form the SG state around $B \parallel c$ for the low magnetic field below B_ϕ .

It is worth noticing that the n -value is almost flat in the angular region between -20° and $+15^\circ$ at 3 T, being the shape like a table mountain volcano. The upward shift in the n -value centered at $B \parallel c$ suggests that the crossing of CDs with $\theta_i = \pm 30^\circ$ suppresses thermal motion of flux lines between neighboring CDs, which is one of the splay effect [8]. The splay effect, moreover, equally occurs within the wide angular-range between -20° and $+15^\circ$. For $\theta = -30^\circ$ or $+30^\circ$ ($B \parallel$ CDs), on the other hand, the n -value slightly decreases compared with that for $B \parallel c$. This implies that the SG state no longer develops at $B \parallel$ CDs: instead of the crossed CDs, the compound PCs consisting of CDs and random defects becomes dominant for the flux pinning in the angular range of $\theta \geq 30^\circ$, which induce a broad peak of J_c centered at $B \parallel c$ for Cr30.

When the magnetic field increases over the matching field 3 T, the J_c peak around $B \parallel c$ diminishes and ends up disappearing at 7 T. The flux pinning by CDs in high magnetic fields above B_ϕ can be explained by the collective correlated pinned glass model [23]: the interstitial flux lines locating in between flux lines directly pinned by CDs are indirectly pinned through the collective interaction with the directly pinned flux lines. According to this model, the disappearance of J_c peak in high magnetic fields is attributed to a weakening in the collective correlated pinning by the dispersion in directions of CDs, since the collective interaction is unstable due to the fluctuation of the direction of flux lines pinned by the direction-dispersed CDs [24]. Note that there is no peak for both the J_c and the n -value even at $B \parallel$ CDs, where flux lines are aligned along one of the two parallel CD families. Since the density of CDs parallel to the magnetic field is one half of $B_\phi = 3$ T, flux lines outnumber the CDs parallel to the magnetic field, even at $B = 3$ T for Cr30. Another family of CDs, on the other hand, is tilted at 60° relative to the magnetic field: the interstitial flux lines interact with the tilted CDs, so that the collective correlation between the interstitial flux lines and flux lines pinned by CDs directly is weakened. Thus, the collective correlated pinned glass state is hardly formed even at $B \parallel$ CDs for Cr30, where kinks of flux lines formed by the pinning interaction with the tilted CDs can easily move along the tilted CDs [25], as shown in figure 3(a). The experimental indication of the kink sliding motion is a non-correlation between J_c and n -value [14, 26], which can be seen in figure 2: the n -value behaves as a concave curve around $B \parallel c$ in high magnetic fields, whereas the angular curve of J_c have a convex curvature.

For $B \parallel ab$, the J_c peak is maintained up to 7 T, which originates from stacking faults and/or the intrinsic pinning due to CuO_2 planes. The n -value, on the other hand, rapidly drops at $B \parallel ab$, where the value of n is approximately 9. Such inverse correlation between J_c and n -value around $B \parallel ab$ can be seen for pure REBCO films in usual, which originates from the kinked vortex structure consisting of pancake vortices and the Josephson segments on the intrinsic PCs [14, 15]. For YBCO, the kinked vortex structure emerges for angles $|\Theta| < \Theta_1$, with $\tan \Theta_1 = d/\xi_{ab}$, where Θ is the angle between the ab -plane and the magnetic field, d is the spacing between CuO_2 planes, and ξ_{ab} is the coherence length in the ab -plane [12]. According to the relations, we obtain $\Theta_1 = 22.9^\circ$, i.e. the kinked vortex is formed at $\theta > 67.1^\circ$ for Cr30 at 60 K, which roughly coincides with the angle region where the n -value shows a dip around $B \parallel ab$. These results indicates that the flux line dynamics around $B \parallel ab$ is substantially affected by the intrinsic PCs rather than by the crossed CDs: the crossing angle of $\theta_i = \pm 30^\circ$ is the obtuse angle of $\pm 60^\circ$ relative to the ab -plane, which is so large that the crossed CDs cannot interact with the flux lines for $B \parallel ab$ [16, 17].

We turn now to consider the angular behaviors of J_c and n -value for Cr60 with $\theta_i = \pm 60^\circ$, which is the acute angle of $\pm 30^\circ$ relative to the ab -plane. Both the J_c and the n -value are significantly different angular-behaviors from those of Cr30, as shown in figure 4: no single peak emerge around $B \parallel c$ for all magnetic fields. The concave angular-curve of the J_c around $B \parallel c$ suggests that there is no correlated pinning along the c -axis for Cr60. We previously reported that CDs crossing at $\theta_i \geq \pm 45^\circ$ work as uncorrelated PCs at $B \parallel c$ rather than as correlated ones, since the pinned segment of flux line on the largely tilted CDs is very short [10]. Hence, the crossed CDs with $\theta_i = \pm 60^\circ$ induce not the entangled state of flux lines but the VG state around $B \parallel c$.

For $B \parallel$ CDs, i.e. $\theta = \pm 60^\circ$, on the other hand, two maxima persist up to 7 T for both the J_c and the n -value, which differs from no peak behavior for Cr30 at $B \parallel$ CDs especially in high magnetic fields. The difference in the flux pinning by the crossed CDs at $B \parallel$ CDs between Cr30 and Cr60 is attributed to the anisotropy of the line tension energy of flux lines. In anisotropic superconductors such as high- T_c materials, the line tension energy of flux lines $\varepsilon_l(\Theta)$ is given by the following equation [1]:

$$\varepsilon_l(\Theta) \propto \varepsilon_0 / \gamma^2 \varepsilon(\Theta)^3, \quad (1)$$

where ε_0 is a basic energy scale, γ is the mass anisotropy, and $\varepsilon(\Theta) = (\sin^2 \Theta + \gamma^{-2} \cos^2 \Theta)^{1/2}$. According to this model, flux lines are hardly elastically deformed around $B \parallel ab$ where the line tension becomes strong. Thus, the single kinks of flux lines between CDs, which can easily move along tilted CDs, are hardly formed through the CDs tilted around the ab -plane for Cr60: flux lines directly or indirectly interact only with the CDs parallel to the magnetic field, as shown in figure 3(b). Therefore, the collective correlated pinned glass state can be formed at $B \parallel$ CDs for Cr60, resulting in the appearance of the two maxima for both J_c and n -value even in high magnetic fields.

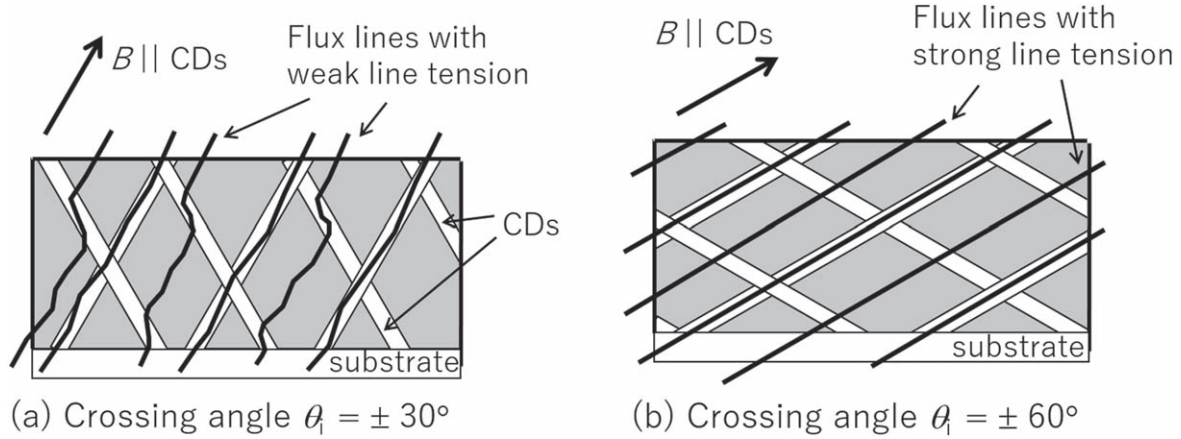


Figure 3. Schematic image of flux pinning at $B \parallel$ CDs for high magnetic field ($>B_\phi$) in the presence of CDs crossing at (a) $\theta_i = \pm 30^\circ$ and (b) $\theta_i = \pm 60^\circ$.

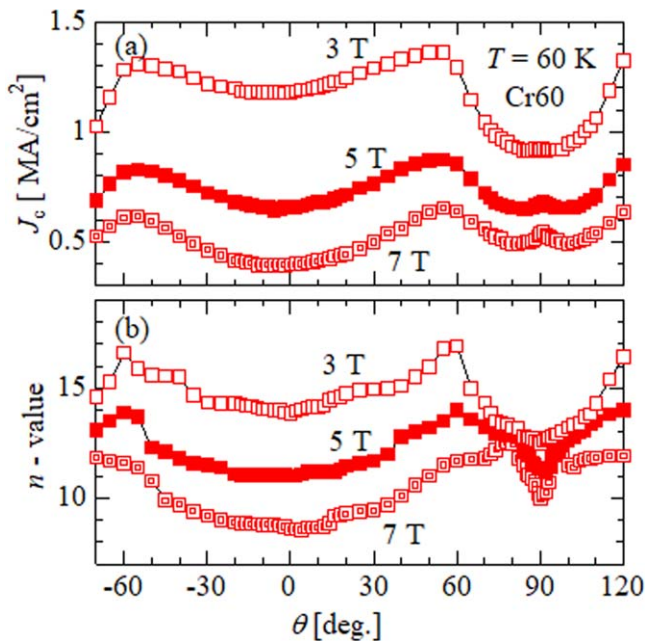


Figure 4. Angular dependence of (a) critical current density J_c and (b) n -value at 60 K for various magnetic fields in YBCO films with (a) $\theta_i = \pm 60^\circ$, Cr60.

As the magnetic field direction approaches $\theta = 90^\circ$, both the J_c and the n -value rapidly decrease in any magnetic field: the CDs crossing at $\pm 30^\circ$ relative to the ab -plane seem to hardly contribute to the improvement of flux pinning at $B \parallel ab$. This is in contrast with the peak behaviors of the J_c and the n -value centered at $B \parallel c$ for Cr30. A J_c peak at $B \parallel ab$ can be slightly seen in high magnetic fields (≥ 5 T), which is attributed to the intrinsic pinning and/or the stacking faults. In addition, a shallow dip in the n -values also occurs at $B \parallel ab$ in the high magnetic fields. That is, the inverse correlation between J_c and n -value slightly exist even for Cr60. The presence of the inverse correlation between J_c and n -value suggests that the flux lines behaves as the kinked vortices around $B \parallel ab$ at 60 K for Cr60. The reason why the flux pinning around $B \parallel ab$ is hardly affected by the crossed CDs not only with $\theta_i = \pm 30^\circ$ but also with $\theta_i = \pm 60^\circ$ is the

anisotropic line tension energy of the kinked vortices, which is roughly identical with those of the continuous Abrikosov vortices as equation (1) [1]. That is, the line tension energy becomes maximum at $B \parallel ab$ even for the kinked vortex structure, so that the flux lines around $B \parallel ab$ can be hardly localized even on the CDs crossing at the acute angle.

Note that the inverse correlation between J_c and n -values for Cr60 is smaller than that for Cr30. One reason for the difference between Cr30 and Cr60 is more irradiation damage on the CuO_2 planes for Cr60. It has been reported that the dip in the n -values at $B \parallel ab$ disappears when the CuO_2 plane texture of films deteriorates [14]. Another possible reason is that the crossed CDs crossing at $\theta_i = \pm 60^\circ$ may slightly suppress the channeling of the stair-case vortex motion along the CuO_2 planes.

To investigate the interaction between the crossed CDs and the angle-dependent structure of flux lines in the liquid state, the angular dependence of flux flow resistivity ρ as a function of temperature at 1.5 T, is given in figure 5. The depression in ρ can be observed in the angular region between -30° and 30° for Cr30 up to 86.5 K, where the values of ρ indicate approximately a constant. The broad depression in ρ centered at $B \parallel c$ monotonously disappears without showing local dips at the irradiation angles as the temperature is increased. The reduction of ρ comes from partially entangled liquid state of flux lines on correlated PCs [27]. Thus, the depression in ρ between the irradiation angles suggests that the entangled liquid state is induced equally over the angular range between -30° and 30° , which roughly coincides with the flat angular region of the n -value in figure 2(b).

For Cr60, the angular curves of ρ take a dome-like shape around $B \parallel c$, while the depressions in ρ occur locally around $B \parallel$ CDs, i.e. $\theta = \pm 60^\circ$ for any temperature. In our previous work, a split into two dips in ρ was observed when the crossing angle of CDs was broadened up to $\theta_i = \pm 45^\circ$ [10]. These suggest that the CDs crossing at $\theta_i = \pm 60^\circ$ can no longer induce the partially entangled liquid state of flux lines around $B \parallel c$. In the vicinity of $B \parallel ab$ including $B \parallel$ CDs, on the other hand, there are three dips in ρ apart from each other. This indicates that the tilted CDs with $\theta_i = 60^\circ$, -60° , and

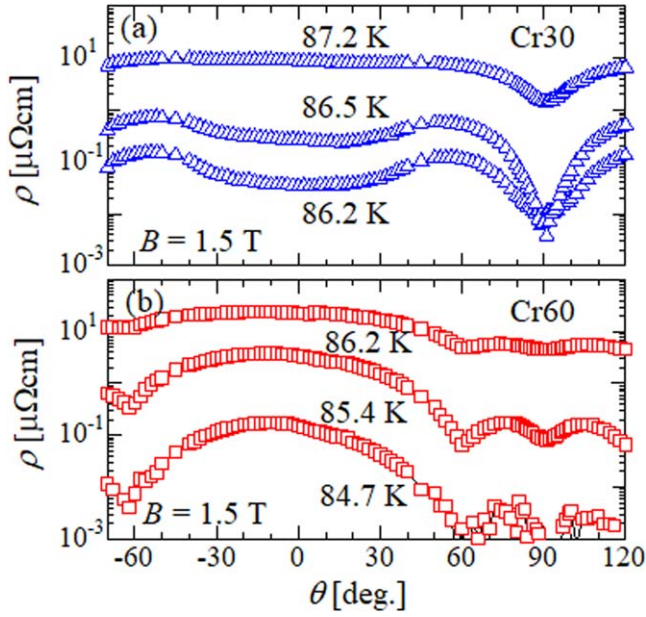


Figure 5. Angular dependence of resistivity ρ at various temperatures and 1.5 T for Cr30 and Cr60, respectively.

the *ab*-correlated PCs act on the liquid state of flux lines, independently of each other. It should be noted that the flux lines around $B \parallel ab$ behave not as the kinked vortex structure but as the continuous vortex structure with an elliptical core in high temperature region such as the liquid state [1, 12]. According to equation (1), the line tension of flux lines for $B \parallel ab$ is stronger than that for $B \parallel c$ even in the liquid state where the line tension weakens [27]. Hence, the motion of flux lines around $B \parallel ab$ are suppressed only by the correlated PCs along the magnetic field: the crossing angle of $\pm 30^\circ$ relative to the *ab*-plane is too large to induce the entangled liquid state at $B \parallel ab$.

Let us now investigate the glass–liquid transition behavior for the angle-dependent structure of flux lines in the presence of the crossed CDs at $B \parallel c$, $B \parallel$ CDs, and $B \parallel ab$. We examine two essential parameters characterizing the glass–liquid transition: one is the VG–liquid transition temperature T_g and another is the dynamic critical exponent z , which characterizes the dynamic behavior of flux lines near the T_g [28]. A type of the glass–liquid transition can be identified from the magnetic field dependent behaviors of T_g and z . The two parameters are evaluated from the critical scaling of the isothermal E – J curves in the vicinity of T_g : the E – J curves collapse on two master curves above and below the T_g , when these are plotted as $(E/J)/|T - T_g|^{\nu(z-1)}$ versus $J/|T - T_g|^{2\nu}$ (ν : static critical exponent) [29]. Figure 6 shows the plot of the scaling collapse of the E – J curves of Cr60 at $\theta = 60^\circ$ for 3 T, where $T_g = 81.7$ K, $z = 9.10$, and $\nu = 1.35$ are obtained: the inset of figure 6 shows a series of E – J curves which are original data used for the critical scaling analysis.

Figure 7 represents the magnetic field dependence of z and the T_g – B phase diagrams in various magnetic field directions, i.e. at $B \parallel c$, $B \parallel$ CDs, and $B \parallel ab$. For $B \parallel c$, Cr30 shows a peak behavior of z and an upturn kink on the T_g – B lines around $B = 1$ T which corresponds to $B_\phi/3$. The two

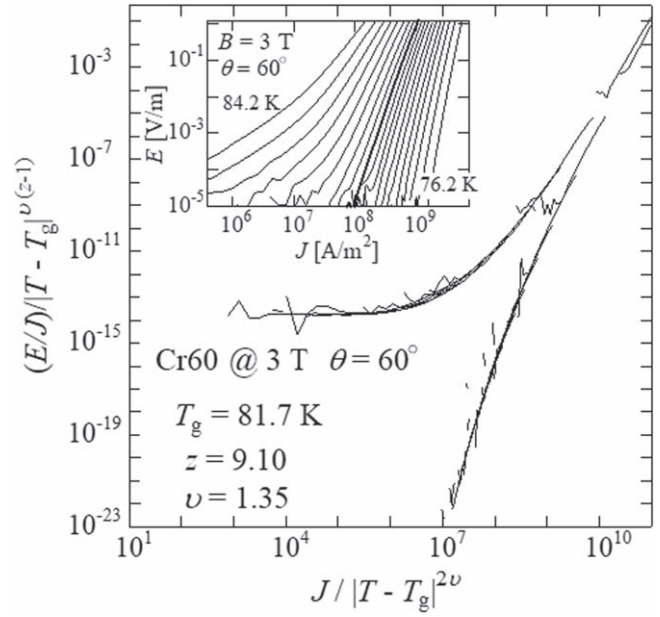


Figure 6. Scaling collapses of E – J curves at 3 T and $\theta = 60^\circ$ for Cr60. Inset: a series of E – J curves of Cr60 at 3 T and $\theta = 60^\circ$ for various temperatures from 76.2 to 84.2 K, which are used in the critical scaling analysis. The bold line denotes the E – J curve at $T_g = 81.7$ K.

characteristic behaviors are strong indicators of the correlated pinning state for the following reasons: at low magnetic fields below $B_\phi/3$, uncorrelated PCs, which are naturally occurring defects in as-grown YBCO films, trap the some parts of flux lines apart from the CDs; when the flux line lattice is matched with randomly distributed CDs at $B \sim B_\phi/3$, the flux pinning by CDs is remarkable and the correlated pinned vortex state (i.e. the SG state in this work) is stably established [30]; this leads to the upward shift of the T_g – B line and the increase of z due to the slower dynamic behavior of flux lines near T_g by the CD pinning interaction [28, 30]. Thus, the crossed CDs with $\theta_i = \pm 30^\circ$ induce the correlated pinned state of flux lines along the *c*-axis, i.e. the SG state at $B \parallel c$, which is also supported by the angular behaviors of J_c and the flux flow resistivity. For Cr60, on the other hand, the value of z is roughly magnetic field independent and there is almost no kink on the T_g – B line at $B \parallel c$. In addition, the T_g – B line in figure 7(d) varies as a function of the reduced temperature as $(1 - T_g/T_c)^\alpha$ with $\alpha = 1.25$, which almost coincides with $\alpha = 4/3$ for uncorrelated pinning regime, i.e. the VG state [31]. Therefore, the crossed CDs with $\theta_i = \pm 60^\circ$ do not work as correlated PCs along the *c*-axis, so that the dynamics of flux lines near T_g is in accordance with the VG model.

For $B \parallel$ CDs, both Cr30 and Cr60 exhibit a clear upturn kink on the T_g – B line in figure 7(e). The characteristic field, at which T_g shows the upturn kink, is approximately $B_\phi(\theta_i)/3$, where $B_\phi(\theta_i)$ is the matching field corresponding to the density of the CDs along the irradiation direction (e.g. $B_\phi(\theta_i = 60^\circ) = B_\phi/2 \cdot 1/\cos 60^\circ = 3$ T). For the magnetic field dependence of z in figure 7(b), on the other hand, the value of z shows a tendency to steeply change around the $B_\phi(\theta_i)/3$ for both samples, whereas a peak or a kink in z is not

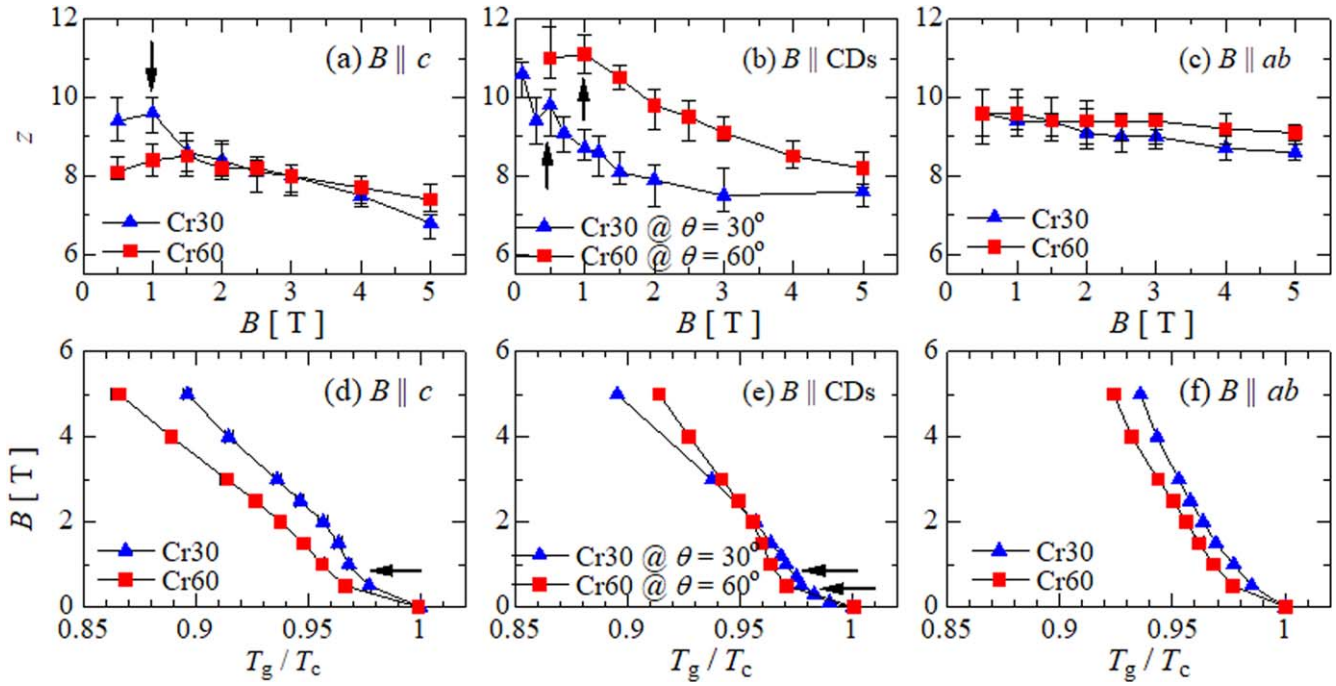


Figure 7. Magnetic field dependence of z and T_g - B phase diagrams at $B \parallel c$ (a) and (d), $B \parallel$ CDs (b) and (e), and $B \parallel ab$ (c) and (f), respectively. The arrows indicate the peak (or the kink) on the z - B curve and the upturn kink on the T_g - B line, respectively.

greater than the error bar, especially for Cr30. These facts suggest that the BG state is induced by one of the two parallel CD families crossing each other. Note that another parallel CD family exists in both the samples, which is largely tilted relative to the magnetic field at $B \parallel$ CDs. For Cr30, the largely tilted CDs induce the kink sliding motion of flux lines for $B > B_\phi(\theta_i)/3$, which leads to faster dynamics of flux lines near T_g , i.e. the abrupt decrease in z for $B > 1$ T. For Cr60, on the other hand, relatively weak field dependence of z can be seen in figure 7(b), suggesting less influence of the largely tilted CDs because of the strong line tension of flux lines at $\theta = 60^\circ$.

In the case of $B \parallel ab$, z and T_g show no features peculiar to the correlated flux pinning for both Cr30 and Cr60: the value of z is not only constant against the magnetic field variation but also approximately same between the samples; the T_g - B lines are monotonous curves without no kink. These results strongly support that the crossed CDs do not work as correlated PCs along the ab -plane for $\theta_i = \pm 60^\circ$, let alone for $\theta_i = \pm 30^\circ$. It has been reported that the VG state develops not only at $B \parallel c$ but also at $B \parallel ab$ in pure YBCO films [32]. The same values of z between Cr30 and Cr60 suggest the universal behavior of the VG state for flux lines with elliptical core shape.

Note that the T_g - B lines at $B \parallel ab$ are in accordance with a power law behavior as $(1 - T_g/T_c)^\alpha$. The values of α are 1.65 for Cr30 and 1.80 for Cr60, respectively. For YBCO single crystals, by contrast, the value of α is 1.24–1.38 at $B \parallel ab$ [33, 34]. The value of α is 1.90–2.10 when CDs are installed along the c -axis for YBCO crystals [33, 35]: the introduction of CDs parallel to the c -axis, which do not contribute to the improvement of flux pinning at $B \parallel ab$, tends to increase the value of α . The values of α for both Cr30 and

Cr60, on the other hand, are between the value of α for the unirradiated crystals and that for the irradiated ones. Although there is no complete correlation between the value of α and the tilt angle of CDs relative to the c -axis, the increase of α may be related to the creation of channels for flux creep motion between the layers by CDs directed close to the c -axis. The clear reason for the difference in α between Cr30 and Cr60 is still now open question.

It is noteworthy that the influence of the crossed CDs on the glass-liquid transition in various magnetic field directions is consistent with the angular behaviors of J_c and the flux flow resistivity. In other words, the influence of the crossed CDs on the dynamics of flux lines does not essentially differ between the thermodynamic states of flux lines, i.e. the glass state and the liquid one in any direction of magnetic field.

4. Conclusions

In order to clarify the pinning mechanism of crossed CDs for the angle-dependent structure of flux lines around the ab -plane, we compared the two configurations of crossed CDs, which were installed into YBCO films at the crossing angle $\pm\theta_i$ relative to the c -axis by using 200 MeV Xe ion irradiation: one configuration is the crossed CDs with $\theta_i = \pm 30^\circ$ and another is with $\theta_i = \pm 60^\circ$. For $B \parallel c$, a J_c peak occurs for $\theta_i = \pm 30^\circ$, suggesting that the entanglement of flux lines is induced by the crossed CDs. For $B \parallel ab$, by contrast, the J_c is hardly affected by the crossed CDs not only with $\theta_i = \pm 30^\circ$, but also with $\theta_i = \pm 60^\circ$. Furthermore, there is no fingerprint of the correlated pinning at $B \parallel ab$ for the behaviors of the dynamic critical exponent z and the glass-liquid transition temperature T_g . When the magnetic field is parallel to one of

the two parallel CD families crossing each other (i.e. at $B \parallel$ CDs), the BG behavior comes out in low magnetic fields for both $\theta_i = \pm 30^\circ$ and $\theta_i = \pm 60^\circ$. In high magnetic fields for $B \parallel$ CDs, on the other hand, the collective correlated pinning state develops only for $\theta_i = \pm 60^\circ$. These results come from the flux line structure with strong line tension around $B \parallel ab$, so that not only the entanglement of flux lines at $B \parallel ab$ but also single kinks of flux lines between the tilted CDs at $B \parallel$ CDs are hardly formed by CDs tilted around the ab -plane.

Acknowledgments

This work was performed by the Common-Use Facility Program of JAEA and was supported by JSPS KAKENHI (JP16K06269) from the Japan Society for the Promotion of Society.

ORCID iDs

Tetsuro Sueyoshi  <https://orcid.org/0000-0003-0925-3971>

References

- [1] Blatter G, Feigelman M V, Geshkenbein V B, Larkin A I and Vinokur V M 1994 *Rev. Mod. Phys.* **66** 1125
- [2] Awaji S, Namba M, Watanabe K, Kai H, Mukaida M and Okayasu S 2012 *J. Appl. Phys.* **111** 013914
- [3] Hua J, Welp U, Schlueter J, Kayani A, Xiao Z L, Crabtree G W and Kwok W K 2010 *Phys. Rev. B* **82** 024505
- [4] Civale L, Marwick A D, Worthington T K, Kirk M A, Thompson J R, Krusin-Elbaum L, Sun Y, Clem J R and Holtzberg F 1991 *Phys. Rev. Lett.* **67** 648
- [5] Matsumoto K, Horide T, Osamura K, Mukaida M, Yoshida Y, Ichinose A and Horii S 2004 *Physica C* **412–414** 1267
- [6] Nelson D R and Vinokur V M 1993 *Phys. Rev. B* **48** 13060
- [7] Fisher D S, Fisher M P A and Fuse D A 1990 *Phys. Rev. B* **43** 130
- [8] Hwa T, Doussal P L, Nelson D R and Vinokur V M 1993 *Phys. Rev. Lett.* **71** 3545
- [9] Kaneko K *et al* 2010 *J. Appl. Phys.* **108** 063901
- [10] Sueyoshi T, Sogo T, Nishimura T, Fujiyoshi T, Mitsugi F, Ikegami T, Awaji S, Watanabe K, Ichinose A and Ishikawa N 2016 *Supercond. Sci. Technol.* **29** 065023
- [11] Sueyoshi T, Nishimura T, Fujiyoshi T, Mitsugi F, Ikegami T and Ishikawa N 2016 *Supercond. Sci. Technol.* **29** 105006
- [12] Berghuis P, Bartolomeo E D, Wagner G A and Evetts J E 1997 *Phys. Rev. Lett.* **79** 2332
- [13] Yamasaki H, Ohki K, Yamada H, Nakagawa Y and Mawatari Y 2008 *Supercond. Sci. Technol.* **21** 125011
- [14] Civale L, Maiorov B, MacManus-Driscoll J L, Wang H, Holesinger T G, Foltyn S R, Serquis A and Arendt P N 2005 *IEEE Trans. Appl. Supercond.* **15** 2801
- [15] Awaji S, Ishihara R, Watanabe K, Shikimachi K, Hirano N and Nagaya S 2011 *Appl. Phys. Express* **4** 013101
- [16] Sueyoshi T, Furuki Y, Kai T, Fujiyoshi T and Ishikawa N 2014 *Physica C* **504** 53
- [17] Sueyoshi T, Iwanaga Y, Fujiyoshi T, Takai Y, Mukaida M, Kudo M, Yasuda K and Ishikawa N 2017 *IEEE Trans. Appl. Supercond.* **27** 8001305
- [18] Zhu Y, Cai Z X, Budhani R C, Suenaga M and Welch D O 1993 *Phys. Rev. B* **48** 6436
- [19] Nakashima K, Chikumoto N, Ibi A, Miyata S, Yamada Y, Kubo T, Suzuki A and Terai T 2007 *Physica C* **463–465** 665
- [20] Strachan D R, Sullivan M C, Fournier P, Pai S P, Venkatesan T and Lobb C J 2001 *Phys. Rev. Lett.* **87** 067007
- [21] Sullivan M C, Strachan D R, Li S, Xu H, Segawa K, Ando Y, Anlage S M and Lobb C J 2008 *Physica C* **468** 284
- [22] Zeldov E, Amer N M, Koren G, Gupta A, McElfresh M W and Gambino R J 1990 *Appl. Phys. Lett.* **56** 680
- [23] Awaji S, Namba M, Watanabe K, Miura M, Yoshida Y, Ichino Y, Takai Y and Matsumoto K 2007 *Appl. Phys. Lett.* **90** 122501
- [24] Awaji S *et al* 2008 *J. Phys.: Conf. Ser.* **97** 012328
- [25] Schuster T, Indenbom M V, Kuhn H and Kronmuller H 1994 *Phys. Rev. B* **50** 9499
- [26] Awaji S, Namba M, Watanabe K, Miura M, Yoshizumi M, Izumi T and Shiohara Y 2010 *Supercond. Sci. Technol.* **33** 014006
- [27] Figueras J, Puig T, Obradors X, Kwok W K, Paulius L, Crabtree G W and Deutscher G 2006 *Nat. Phys.* **2** 402
- [28] Reed D S, Yeh N-C, Jiang W, Kriplani U, Konczykowski M and Holtzberg F 1996 *Int. J. Mod. Phys. B* **10** 2723
- [29] Koch R H, Foglietti V, Gallagher W J, Koren G, Gupta A and Fisher P A 1989 *Phys. Rev. Lett.* **63** 1511
- [30] Nojima T, Katakura M, Okayasu S and Kobayashi N 2002 *Physica C* **378–381** 593
- [31] Gammel P L, Schneemeyer L F and Bishop D J 1991 *Phys. Rev. Lett.* **66** 953
- [32] Woltgens P J M, Dekker C, Swuste J and Wijn H W 1993 *Phys. Rev. B* **48** 16826
- [33] Paulius L M, Fendrich J A, Kwok W K, Koshelev A E, Vinokur V M and Crabtree G W 1997 *Phys. Rev. B* **56** 913
- [34] Petrean A, Paulius L, Tobos V, Cronk H and Kwok W K 2014 *Physica C* **505** 65
- [35] Krusin-Elbaum L, Civale L, Blatter G, Marwick A D, Holtzberg F and Field C 1994 *Phys. Rev. Lett.* **72** 1914